Radial Force Control of Multi-Sector Permanent Magnet Machines

G. Valente, L. Papini, A. Formentini, C. Gerada, P. Zanchetta

***Abstract* -- The paper presentsn alternative radial force control technique for a Multi-Sector Permanent Magnet machine (MSPM). Radial force control has been widely investigated for a variety of bearingless machines and can be also applied to conventional PMSM aiming the reduction of the mechanical stress on the bearings as well as reduce the overall vibration. Traditional bearingless motors rely on two independent sets of windings dedicated to torque and suspension respectively. The work presented in this paper takes advantage of the spatial distribution of the winding sets within the stator structure towards achieving a controllable net radial force. In this paper the α-β axis model for the MSPM and the theoretical investigation of the force production principle is presented. A novel force control methodology based on the Single Value Decomposition (SVD) technique is described. The predicted performances of the MSPM have been validated using Finite Element simulations and benchmarked against state of the art control techniques.**

***Index Terms*-- Bearingless Multi-Sector Permanent Magnet machines, Radial Force Control, Singular Value Decomposition (SVD), Pseudo inverse matrix, Vibration Damping.**

I. Introduction

Permanent magnet synchronous machines (PMSM) are widely adopted in many high performance industrial applications and more recently have seen an increased uptake driven by transportation including automotive, railway, marine and aerospace [1]. Application requirements vary from case to case, however there is a general trend towards increasing the power density and the efficiency of the electrical machine aiming a reduction of the system fuel consumption, emission and range. Longer lifetime, lower maintenance, higher reliability and lower noise machines are often critical aspects in hybrid and full electric automotive applications. The reliability of electrical machines and maintenance requirements are typically strongly affected by the bearings [2]. Active control of the radial forces that take place in the electrical machines could lead to significant improvement in noise reduction and vibration dampening. This would also enable the compensation of external forces acting on the rotating structure such as unbalance magnetic pull (UMP), inertial forces and forces of other nature. The relatively high failure rate of mechanical bearing as well as the oil-free requirement of some applications has pushed the development of bearingless PMSM. As a matter of fact, magnetic levitation enables the potential of full rotor-dynamic control on the rotating component which could allow the achievement of very high rotational speeds [3] and provide damping effects while crossing critical frequencies. Bearingless technology applied to electrical machines has been used widely in high performance industrial environments for high speed [1] and oil-free applications [2]. Rotor levitating technology is most commonly achieved by applying Active Magnetic Bearings (AMB) as well as Passive Magnetic Bearings (PMB) whilst the electrical machine is typically designed to optimize torque production and minimize torque ripple and vibration [4]. AMBs and PMBs unfortunately lead to an increased overall length, higher weight and higher cost.

More recently, bearingless PMSM technology has been proposed in order to embed the characteristic of AMBs or PMBs into the motor structure [3]. Therefore, bearingless PMSM allows enhancing the reliability, maximizing the power to weight ratio as well as the power to volume ratio.

The x-y forces and the torque developed by the electrical motor can be independently controlled adopting two sets of windings [5]. However, adopting an *"ad hoc"* winding arrangement, it is possible to merge the force and torque control. In [6], the geometrical arrangement of the winding structure, formed by three winding sectors, enables the control of the torque as well as the net radial force through the independent d-q axis current control of each sector. In a similar way in [7], the force and torque produced in a multiphase slice permanent magnet bearingless motor are controlled by solving an optimization problem that minimizes the power losses in the machine.

In the proposed work, an alternative radial force and torque control is applied to a MSPM. The effectiveness of the control technique proposed is validated through Finite Element Analysis (FEA). A multi-sector three-phase MSPM machine is considered in this work, consisting in a conventional 18 slot – 6 poles PMSM but with a re-arranged winding configuration. The multi-three phase structure features a spatial distribution of the conductors in order to achieve an independent control of x-y forces and of torque over a discrete number of sectors. The current components are controlled by adopting a set of conventional three phase inverter in combination with a single control platform. The impact of the control strategy is the focus of this work. A computationally efficient control technique based on the minimization of copper losses is presented. The modelling and characterization of the MSPM machine is developed in combination with the force/torque control technique. The mathematical model considered suggests the investigation of control techniques that account for the cross-coupling effect in the torque and force capabilities of the system. The current control reference signals are evaluated adopting the SVD technique which is compared with the state of the art

G. Valente , L. Papini, A. Formentini, C. Gerada, P. Zanchetta, are with the PEMC group, University of Nottingham, Nottingham, NG7 2RD, UK (e-mail: eexgv@exmail.nottingham.ac.uk)

control strategies proposed in literature.

II. Multi-Sector Permanent Magnet Machines

A. The machine structure

In Fig. 1, the cross section of the MSPM machine considered in this work is presented. The multi-three phase winding arrangement is highlighted. The main characteristics of the surface mounted PM machine are listed in Table I. Each of the three phase sectors have a full-pitched distributed winding with a floating star point. The independent current control for each sector allows for both torque and radial force control.

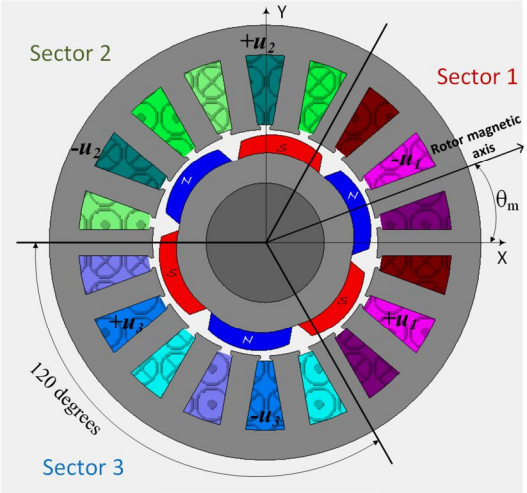

Fig. 1. 18 slot – 6 poles – 3 sectors PMSM distributed winding considered.

Table I
Machine Parameters

Parameter	Value
Pole number ($2p$)	6
PM material	NdFeB
kW Rating	1.5 kW
Turn/coil	22
No Load Flux/sector (${}^{s}\varphi_0$)	0.026 Wb
Rated Speed (ω_m)	3000 rpm
Torque constant (k_T)	0.128 Nm/A
Voltage constant (k_V)	6.022 V/krpm
Phase resistance (R_{ph})	0.0808 Ω
d-axis Inductance/sector (${}^{s}L_d$)	0.445 mH (@ 1 A)
q-axis Inductance/sector (${}^{s}L_q$)	0.442mH (@ 1 A)
Geometrical Parameters	
Outer Stator diameter	95 mm
Axial length	91 mm
Air-gap length	1 mm
Magnets thickness	4 mm

B. The mathematical model

The mathematical model of the torque-force characteristic of the presented machine is derived in a generic form that can be extended to every MSPM machine. Under the assumptions of linear magnetic behavior of the materials, magnetic decoupling between sectors and taking advantage of the geometrical and electromagnetic symmetries featured, only one machine sector is considered and the superposition principle is applied. The machine under investigation has a number of sectors $n_s = p$ which are assumed to be magnetically decoupled. The left superscript s on the introduced quantities of this manuscript is adopted in order to relate the quantities discusses with the single s^{th} sector. The total torque T_E results as the algebraic sum of the torque developed by each single sector s: $T_E = \sum {}^{s}T_E$. Similarly, the total vector of force $\vec{F}_E$ acting on the rotor results as the vector sum of the forces developed by each sector s: $\vec{F}_E = \sum {}^{s}\vec{F}_E$. Based on the orthogonal decomposition of the force vectors, the total sum can be expressed as the sum of the orthogonal components respectively ($F_{E,x} = \sum {}^{s}F_{E,x}$; $F_{E,y} = \sum {}^{s}F_{E,y}$). The simplified model proposed does not account for rotor position variation as it is assumed to be rigid, centered and radially fixed by stiff mechanical ball-bearings. Further considerations can be done to include the effect of rotor displacement in the x-y plane. The torque and the forces developed by s^{th} sector of the machine are therefore considered as a function of the stationary reference frame current components ${}^{s}i_\alpha$ and ${}^{s}i_\beta$ of each sector, the electrical angular position θ_e ($\theta_e = p\theta_m$) of the rotor magnetic axis with respect the winding magnetic axis and the geometrical angular position ${}^{s}\gamma$ of the windings magnetic axis with respect the reference X-axis angular position. Introducing the electromagnetic wrench vector ${}^{s}\overline{\boldsymbol{W}}_E$ [8] of each sector, defined by piling the force components ${}^{s}F_{E,x}$ and ${}^{s}F_{E,y}$ and the electromagnetic torque ${}^{s}T_E$, the matrix formulation (1) express the mechanical output state function for the s^{th} sector of the machine

$$ {}^{s}\overline{\boldsymbol{W}}_E = {}^{s}\boldsymbol{K}_E(\theta_e, {}^{s}\gamma)\, {}^{s}\bar{I}_{\alpha\beta} = {}^{s}\boldsymbol{K}_E(\theta_e, {}^{s}\gamma) \begin{bmatrix} {}^{s}i_\alpha \\ {}^{s}i_\beta \end{bmatrix} \quad \textbf{(1)} $$

where ${}^{s}\boldsymbol{K}_E$ is the matrix that characterizes the electro-magneto-mechanical output through mapping the current to x-y force and torque coefficients while ${}^{s}\bar{I}_{\alpha\beta}$ is the vector of the α-β axis currents of sector s. The matrix ${}^{s}\boldsymbol{K}_E$ can be expressed as (2).

$$ {}^{s}\boldsymbol{K}_E(\theta_e, {}^{s}\gamma) = \begin{bmatrix} {}^{s}k_{x,\alpha}(\theta_e, {}^{s}\gamma) & {}^{s}k_{x,\beta}(\theta_e, {}^{s}\gamma) \\ {}^{s}k_{y,\alpha}(\theta_e, {}^{s}\gamma) & {}^{s}k_{y,\beta}(\theta_e, {}^{s}\gamma) \\ {}^{s}k_{T,\alpha}(\theta_e) & {}^{s}k_{T,\beta}(\theta_e) \end{bmatrix} \quad \textbf{(2)} $$

The above consists in a set of coefficient ${}^{s}k_{*,\times}$ where $*,\times$ defines the output and the current components, respectively. The elements of the electromagnetic torque sub-matrix ${}^{s}\boldsymbol{K}_{E,T}(\theta_e)$ are defined in (3).

$$ \begin{cases} {}^{s}k_{T,\alpha}(\theta_e) = k_T \sin(\theta_e) \\ {}^{s}k_{T,\beta}(\theta_e) = k_T \cos(\theta_e) \end{cases} \quad \textbf{(3)} $$

The electromagnetic torque defined by (3) is not affected by the parameter ${}^{s}\gamma$ since each sector is considered identical and magnetically independent to the others, therefore featuring the same torque characteristic. On the other hand, the sub-matrix of the electromagnetic forces ${}^{s}\boldsymbol{K}_{E,F}(\theta_e, {}^{s}\gamma)$ developed by the s^{th} sector can be expressed with respect the sub-matrix ${}^{1}\boldsymbol{K}_{E,F}(\theta_e, 0)$ of the reference sector (sector 1 having considered ${}^{1}\gamma = 0$). The compact expression of the

force-torque characteristic of the s^{th} sector of the device is reported in (4), suggesting that only one sector has to be characterized with respect the parameter θ_e to account for the main aspects of the machine.

$$ {}^{s}\boldsymbol{K}_{E}(\theta_e, {}^{s}\gamma) = \begin{bmatrix} \boldsymbol{R}^{T}({}^{s}\gamma)\ {}^{1}\boldsymbol{K}_{E,F}(\theta_e, 0) \\ {}^{s}\boldsymbol{K}_{E,T}(\theta_e) \end{bmatrix} \quad \textbf{(4)} $$

The effect of the geometric position of each sector can be accounted introducing the bi-dimensional rotation matrix $\boldsymbol{R}({}^{s}\gamma)$ expressed in (5) and function of the parameter ${}^{s}\gamma$

$$ \boldsymbol{R}({}^{s}\gamma) = \begin{bmatrix} \cos({}^{s}\gamma) & -\sin({}^{s}\gamma) \\ \sin({}^{s}\gamma) & \cos({}^{s}\gamma) \end{bmatrix};\ {}^{s}\gamma = \frac{2\pi}{s} + \gamma_0 \quad \textbf{(5)} $$

where the expression of the parameter ${}^{s}\gamma$ for an equally spaced sector structure is proposed and γ_0 defines the angular position of the magnetic axis of the reference sector.

C. The machine characterization

Both capabilities and performances of the machine in terms of torque and force production are the topic of this section. The α-β axis components of the no load flux linkage of the generic s^{th} sector are defined according to (6)

$$ \begin{cases} {}^{s}\varphi_{0,\alpha} = {}^{s}\varphi_0 \cos(\theta_e) \\ {}^{s}\varphi_{0,\beta} = {}^{s}\varphi_0 \sin(\theta_e) \end{cases} \quad \textbf{(6)} $$

where ${}^{s}\varphi_0$ is the fundamental of the no load flux linkage with the winding structure. The well-known torque equation under sinusoidal approximation for PM machines [1] is reported in (7) referred to the generic s^{th} sector.

$$ \begin{aligned} {}^{s}T_E &= \frac{3}{2} p \left({}^{s}\varphi_{0,\alpha}\ {}^{s}i_\beta - {}^{s}\varphi_{0,\beta}\ {}^{s}i_\alpha \right) \\ &= \frac{3}{2} p\ {}^{s}\varphi_0 \left(\cos(\theta_e)\ {}^{s}i_\beta - \sin(\theta_e)\ {}^{s}i_\alpha \right) \end{aligned} \quad \textbf{(7)} $$

The torque constant that characterizes the elements of ${}^{s}\boldsymbol{K}_{E,T}(\theta_e)$ in (3) are evaluated according to (7). Fig. 2 presents the comparison of the analytical predicted torque, obtained by (7), and the FE simulation result for the maximum value of current magnitude ${}^{s}I_{\alpha\beta,max} = 13\ [A] \forall s$.

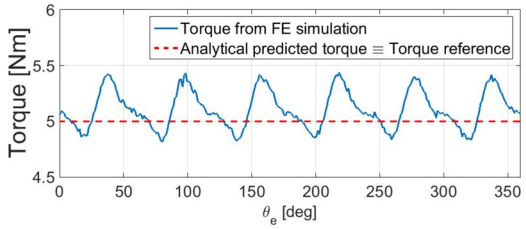

Fig. 2. Torque produced.

The coefficients of the matrix ${}^{1}\boldsymbol{K}_{E,F}(\theta_e, 0)$ introduced in the previous section, characterizes the force capabilities of the device. They are evaluated by means of two FE simulations, feeding only the three-phase winding of the reference sector with constant ${}^{1}i_\alpha = 1\ [A]$, ${}^{1}i_\beta = 0\ [A]$ and ${}^{1}i_\alpha = 0\ [A]$, ${}^{1}i_\beta = 1\ [A]$ respectively, while rotating the rotor by one electrical period. The analytical evaluation of the coefficients of ${}^{1}\boldsymbol{K}_{E,F}(\theta_e, 0)$ is performed and their trend is compared with FE results in Fig. 3. The calculation is carried out through the integration along the airgap circumference of the Maxwell stress tensor equations [9], after the calculation of the radial and tangential components of the flux density in the middle of the airgap. The flux density components are reported in (8) showing the permanent magnet and current winding contributions.

$$ \begin{aligned} B_r(\xi, \theta_e) &= B_{r,PM}(\xi, \theta_e) + {}^{1}B_{r,w}(\xi, \theta_e) \\ B_\vartheta(\xi, \theta_e) &= B_{\vartheta,PM}(\xi, \theta_e) + {}^{1}B_{\vartheta,w}(\xi, \theta_e) \end{aligned} \quad \textbf{(8)} $$

The reference of the angular variable ξ corresponds with the magnetic axis of the reference sector.
$B_{r,PM}$ and $B_{\vartheta,PM}$ are the flux density components produced by the permanent magnets [10], while ${}^{1}B_{r,w}$ and ${}^{1}B_{\vartheta,w}$ are the flux density components produced by the current imposed in the three-phase winding of the reference sector [11]. The sinusoidal approximated expression of the elements of the 2x2 matrix ${}^{1}\boldsymbol{K}_{E,F}(\theta_e, 0)$ is reported in (9)

$$ \begin{cases} {}^{1}k_{x,\alpha}(\theta_e, 0) = \tilde{k}_{x,\alpha} \cos(\theta_e + \varphi_{x,\alpha}) \\ {}^{1}k_{x,\beta}(\theta_e, 0) = \tilde{k}_{x,\beta} \cos(\theta_e + \varphi_{x,\beta}) \\ {}^{1}k_{y,\alpha}(\theta_e, 0) = \tilde{k}_{y,\alpha} \cos(\theta_e + \varphi_{y,\alpha}) \\ {}^{1}k_{y,\beta}(\theta_e, 0) = \tilde{k}_{y,\beta} \cos(\theta_e + \varphi_{y,\beta}) \end{cases} \quad \textbf{(9)} $$

where $\varphi_{*,\times}$ is the phase shift of the force's components.

(6)

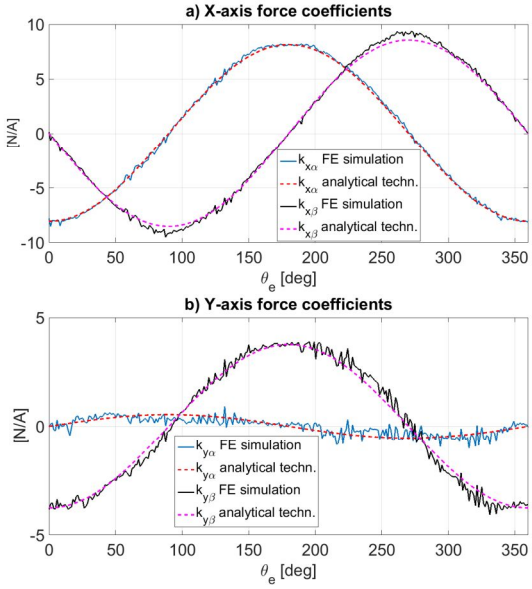

Fig. 3. FE and analytical force coefficient evaluation.

In Table II the coefficients evaluated for the machine under investigation are reported.

Table II
FORCE COEFFICIENTS

	$x-\alpha$	$x-\beta$	$y-\alpha$	$y-\beta$
$\tilde{k}_{*,\times}$	8.1	8.5	0.5	3.9
$\varphi_{*,\times}$	π	$\pi/2$	$-\pi/2$	π

The $3 \times 2n_s$ total matrix that characterizes the electro-magneto-mechanical output of the considered machine is expressed in (10).

$$\boldsymbol{K}_E = \left[{}^1\boldsymbol{K}_E(\theta_e, {}^1\gamma) \ \cdots \ {}^3\boldsymbol{K}_E(\theta_e, {}^3\gamma) \right] \quad \textbf{(10)}$$

$\boldsymbol{K}_E$ in general do not results in a square matrix. In the following section, the problem of the determination of the current reference signal to achieve a stable and reliable control is discussed.

III. RADIAL FORCE CONTROL METHOD

A. *The control method*

The current commands required to control the x-y force and torque can be determined by evaluating the inverse of the matrix $\boldsymbol{K}_E$. However, the number of equations involved is three, which is smaller than the number of state variables ($2n_s$), hence a proper strategy has to be considered in order to obtain reasonable phase current reference signal [7] as the mathematical problems presents an infinite set of possible solutions. Targeting the minimization of the resistive joule losses, the Moore–Penrose pseudo inverse is proposed as the generalization of the inverse of the matrix $\boldsymbol{K}_E$. The performances achieved are benchmarked against an alternative control strategy which is described in the following paragraph.

B. *Decoupled torque and force control technique*

Decoupled models have been considered in [6] to design rotor position control strategies levering on the d-q axis modelling of PMSM machines [1]. The torque demand and the force vector are generated by controlling the n_s q-axis and d-axis components of the current in the synchronous reference frame, respectively. Levering on the magnetically isotropic structure of the MSPM machine, the torque is controlled only by means of the q-axis current components of each sector. The total q-axis current demand is obtained considering the torque expression (11).

$$T_E = \sum_{s=1}^{n_s} {}^s\kappa_T \ {}^s i_q = n_s \, \kappa_T \, i_q \ \Rightarrow \ {}^s i_q = \frac{T_E}{n_s \, \kappa_T} \quad \textbf{(11)}$$

The q-axis current values, obtained by (11), define the input current of the FE model. **Fig. 2** present the torque developed by the machine considering identical current reference for all the sectors and targeting $T_{Nominal} = 5 \ [Nm]$.

In [6], the transformation of the forces developed by each sector to the rectangular forces component on the overall rotor structure is introduced aiming a reduction of the order of the problem. Under the assumption of electromagnetic forces related with only the d-axis currents components, (11)-(12) define the complete model of the MSPM machine

$$\begin{bmatrix} {}^1i_d \\ {}^2i_d \\ {}^3i_d \end{bmatrix} = \frac{2}{3}\frac{1}{k_F} \begin{bmatrix} \cos({}^1\gamma) & \sin({}^1\gamma) \\ \cos({}^2\gamma) & \sin({}^2\gamma) \\ \cos({}^3\gamma) & \sin({}^3\gamma) \end{bmatrix} \begin{bmatrix} F_{E,x} \\ F_{E,y} \end{bmatrix} \quad \textbf{(12)}$$

where k_F is the current-force coefficient.

C. *The force ripple compensation technique*

The rotor structure is considered to be rigid, centered and radially fixed by stiff mechanical ball-bearings as declared in Section II.B. The above assumptions lead to a simplified mechanical rotor model where the external forces $\vec{F}_D$ acting on the mechanical bearing that support the rotating element of the MSPM machine can be considered to be consisting of the rotor weight force vector $\vec{F}_W$ and the intrinsic UMP $\vec{F}_{UMP}$ generated by the electromagnetic and geometric structure. Imposing the mechanical equilibrium of the rotor, the force balance equation (13) is considered including the controllable electromagnetic force $\vec{F}_E$ whose generation is discussed in the previous sections.

$$\vec{F}_W + \vec{F}_{UMP}(\theta_e, \bar{I}_{\alpha\beta}) + \vec{F}_E(\theta_e, \bar{I}_{\alpha\beta}) = 0 \quad \textbf{(13)}$$

The suspension force $\vec{F}_E$ can be controlled in magnitude and phase in order to compensate external forces $\vec{F}_W$ (bearing reaction included) and $\vec{F}_{UMP}(\theta_e, \bar{I}_{\alpha\beta})$ achieving a damping effect of the mechanical stress on the bearings.

The cylindrical components of the electromagnetic forces developed by the MSPM machine are reported in Fig. 4 having defined the supplied current according to (12). The force-torque decoupled (FTD) technique [6] is considered. FE simulations are adopted to compute the resulting force acting on the rotor structure therefore including the UMP developed by means the machine. The influence of the q-axis current on the force production is investigated considering the compensation of the rotor weight force ($F_W = 25 \ [N] \quad \forall\theta_e$) at different torque load conditions. The impact of the q-axis current is mainly found affecting the phase of the vector of the electromagnetic forces (Fig.4.b). The maximum phase variation of $\approx$ 2.5 degrees is shown in Fig. 4 between the no load and torque load condition.

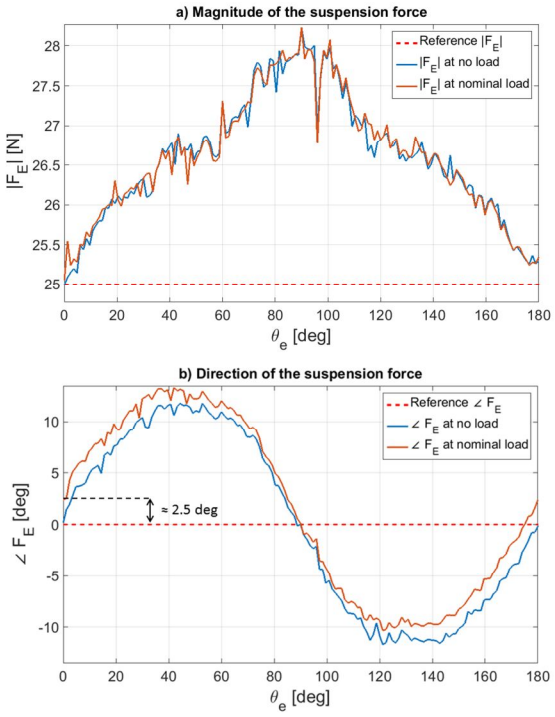

Fig. 4. Suspension force produced at no load and at nominal load adopting FDT technique.

The oscillation in the commanded force component occurs due to the geometric and magnetic structure of the machine, generally referred to as UMP. The compensation of the

aforementioned harmonic component is required in order to reduce the time dependent stress on the bearing element.
In [6] an harmonic compensator is presented as the solution of the highlighted phase error. The ratio of the dynamic force magnitude developed (rotor in motion at constant mechanical speed: $\omega_m = const$) with respect the static force (rotor in stall: $\omega_m = 0$) defines the amplitude gain k_h while the difference between the dynamic and static direction angle represents the angle direction compensation factor Φ_h. The expressions are reported in (14) and (15).

$$k_h(\theta_e) = \frac{|F_E(\theta_e)|}{|F_E(0)|} \tag{14}$$

$$\Phi_h(\theta_e) = \Phi_h(\theta_e) - \Phi_0 \tag{15}$$

The force reference components input of the control system expressed by (12), are corrected by means of a harmonic compensation matrix $\boldsymbol{C}_h(\theta_e)$ defined in [6]. The parameters $k_h(\theta_e)$ and $\Phi_h(\theta_e)$ have to be calculated using FEA. The control strategy therefore presents the harmonic compensator in the form of lookup table as the coefficients require to be updated according to the rotor position and torque load condition in order to guarantee stable operation of the machine. The impact of the torque demand on the generated force is investigated in [12] where FEA are adopted to validate the proposed analytical model.
In the following section a novel control technique to define the current commands of the $n_s$sectors is presented.

D. Pseudo Inverse matrix

The conventional control strategies adopted do not have limitations on the maximum current supplied to each sector. The total current injected in the winding structures has an impact on the magnetic load distribution in the machine as well as the total joule losses which are the major source of heat in electrical machines. The minimization of the losses can have beneficial effect on the overall efficiency of the system, avoiding de-rating due to hotspots as well as reducing the impact of possible magnetic core saturation [13]. The compact expression of the total heat losses is (16)

$$P_{cu} = \bar{I}_{\alpha\beta}^T \, \boldsymbol{R} \, \bar{I}_{\alpha\beta} \tag{16}$$

where $\boldsymbol{R}$ is the matrix of electrical resistances. Under the assumption of identical electrical resistance of the phases, $\boldsymbol{R} = diag(\, R_{ph})$ and therefore (16) reduces to

$$P_{cu} = R_{ph} \, \bar{I}_{\alpha\beta}^T \, \bar{I}_{\alpha\beta} \tag{17}$$

The rectangular matrix $\boldsymbol{K}_E \in R^{3\times 2n_s}$ (10) which describes the input-output correlation of the plant, cannot be inverted with conventional techniques. The Moore–Penrose pseudo inverse is considered as the generalization of the inverse matrix and is commonly applied to compute the solution of under- and over-determined system of linear equations. In the specific configuration considered in this work $n_s = 3$ implying that the system in (10) is underdetermined with an infinite number of solutions. Considering that $\boldsymbol{K}_E$ is full rank for column for every value of θ_e, its pseudo inverse $\boldsymbol{K}_E^+$ can be expressed as in (18).

$$\boldsymbol{K}_E^+ = \boldsymbol{K}_E^T \left(\boldsymbol{K}_E \, \boldsymbol{K}_E^T\right)^{-1} \tag{18}$$

The vector of the current demand required to develop the reference mechanical output $\bar{W}_E^*$ can be there expressed as in (19).

$$\bar{I}_{\alpha\beta}^{\prime} = \boldsymbol{K}_E^+ \, (\theta_e, \, {}^s\gamma) \, \bar{W}_E^* \tag{19}$$

The resulting reference current calculated according to the definition of the generalized inverse, results in that quantity which minimizes (17) by means minimizing the currents, therefore achieving a minimum overall losses operative condition.. The generalized inverse can be computed using the singular value decomposition (SVD) with a reduction of the computational effort needed.
The online computation of the pseudo inverse matrix $\boldsymbol{K}_E^+$ is a difficult task mainly due to the large amount of operation required even if the SVD technique is adopted. Taking advantage of the full characterization of the machine, the single components of the $\boldsymbol{K}_E$ matrix result as known quantities and in this work are considered expressed in their approximated sinusoidal form. The elements of the pseudo inverse matrix $\boldsymbol{K}_E^+$ are therefore evaluated offline reducing drastically the online computation effort needed. The trend of the elements of the matrix K_E^+ with respect the electrical angular position is reported in Fig. 5.

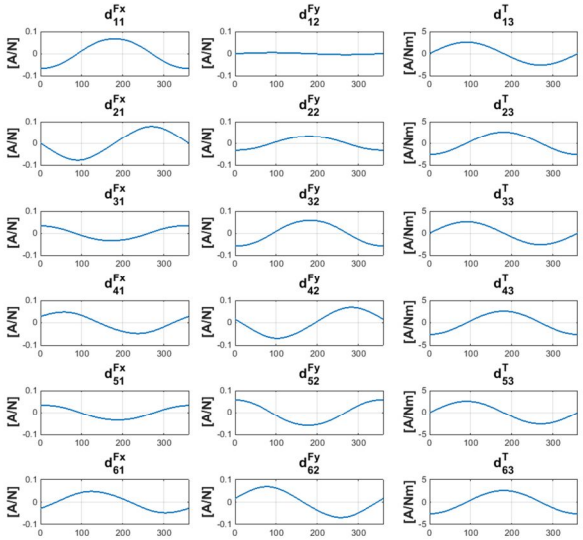

Fig. 5. Coefficients of the Pseudo Inverse matrix $\boldsymbol{K}_E^+$

IV. CONTROL TECHNIQUE COMPARISON

In this section the performance and capabilities of the control strategy proposed are presented and compared with the more conventional ones.
The strategies compared are listed below:

1. The force-torque decoupled (FTD) technique [6]
2. The FTD including the harmonic compensation technique (HFTD) [6].
3. The Pseudo Inverse matrix technique (PIM)

The suspension forces produced adopting the different techniques are evaluated by FE simulations.

Fig. 6 and Fig. 7 present the resultant suspension force produced by the three control strategies considered under no load operating condition ($T_E = 0$). Fig. 6 shows the magnitude $|F_E|$ and the direction $\angle F_E$ obtained commanding $F^*_{E,x} = F_W$ and $F^*_{E,y} = 0$ as force references. In Fig. 7 the x-y force components obtained adopting $F^*_{E,x} = -30$ N and $F^*_{E,y} = 20$ N as force references are illustrated. It is straightforward to notice that both HFTD and PIM perform an effective damping against the UMP while generating the levitating force required compared with the FDT technique. The results validate the proposed technique with respect force production without the adoption of compensation stage or lookup table while relying only on analytical solutions that can be easily implemented.

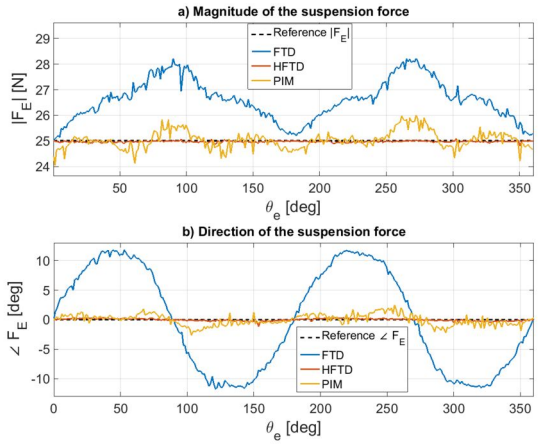

Fig. 6. Force generation with the three considered techniques ($|F_E| = 25$ [N] and $\angle F_E = 0\ [deg]$).

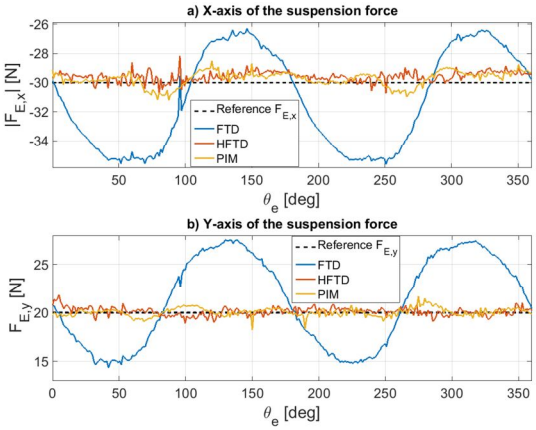

Fig. 7. Force generation with the three considered techniques ($F_{E,x} = -30$ [N] and $F_{E,y} = 20$ [N]).

The effect of commanding $F^*_{E,x} = F_W$ and $F^*_{E,y} = 0$ as force references to the PIM is presented in Fig. 8 under no load and rated load conditions. The developed torque is presented in Fig. 8 c) while the reference forces are applied. It can be noticed that the trends of $|F_E|$ and $\angle F_E$matches for both no load and load conditions. Therefore, the force-torque coupling found for the FTD in Fig. 4 has been remarkably reduced, validating the proposed method.

The quality of the suspension force produced is appreciated observing the Total Harmonic Distortion (THD) of the magnitude $|F_E|$ and the maximum error of the force direction $\angle F_E = \left(\frac{\max(\angle F_E) - (\angle F_E)^{ref}}{360} * 100\right)$. In Fig. 9 the three techniques are compared using the aforementioned parameters. The operating condition reported in Fig. 7 (no load, $F^*_{E,x} = -30$ [N] and $F^*_{E,y} = 20$ [N]) has been selected for this analysis.

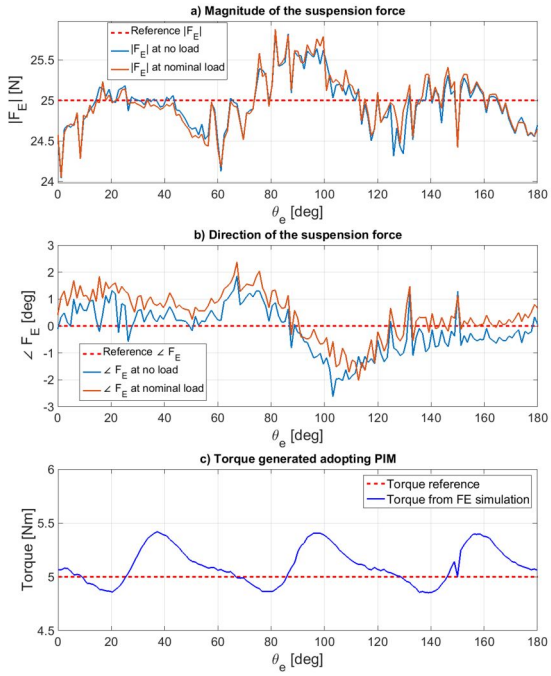

Fig. 8. Suspension force produced with PIM at no load and at nom. load

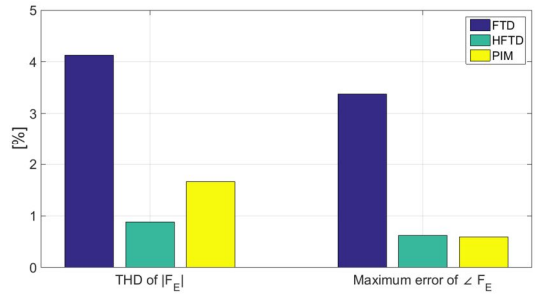

Fig. 9. Magnitude $|F_E|$ THD and phase error comparison between control techniques (for $F_{E,x} = -30$ [N] and $F_{E,y} = 20$ [N]).

From the analysis performed, it can be noticed that both the HFTD and PIM enables to considerably reduce the magnitude THD and the maximum direction error with respect to the FTD. The HFDT technique presents the smallest THD in the force magnitude since it relies on a lookup table that enables to perform a point by point compensation. The PIM technique seats in between the FDT and HFDT control strategies in terms of overall THD while performing comparably with respect the HFTD method for what concerns the maximum error in the force phase angle. However, the lower on-line computational effort required adopting the proposed PIM technique results in a considerable advantage for what concerns direct implementation and generalization of the above compared with HFTD. The influence of the torque production on the

suspension force generation is also accounted in the PIM whereas the FDT technique requires the additional compensation technique (HFDT) to be evaluated.
To summarize, the main features of the radial force control techniques under investigation are qualitatively compared in Table III.

Table III
QUALITATIVE COMPARISON

	FTD	*HFTD*	*PIM*
Force Magnitude	+	+	+
Force Quality	-	+	+
Joule Losses	-	+	+
Computational simplicity	+	-	+

V. CONCLUSIONS

In this paper, the multi-sector motor proposed has been analyzed and a novel mathematical model for the electromagnetic torque and suspension force production has been carried out. The pseudoinverse matrix is introduced to define the current reference signals. The capabilities of the proposed method are validated through FEA for different force and torque operative conditions. The proposed method has been also compared, on the basis of different assessment criteria, with more conventional techniques. The PIM technique is demonstrated to be capable of UMP compensation as well as stable force production without the adoption of compensation stage in the control loop. The output achieved with PIM features higher THD with respect the benchmarked HFDT control strategy. However, the nature of the presented method features notable advantages for its simplicity in the quantities evaluation, low computational effort for online control implementation and results suitable for generalization.

VI. REFERENCES

[1] L. Papini, T. Raminosoa, D. Gerada *et al.*, "A high-speed permanent-magnet machine for fault-tolerant drivetrains," *IEEE Trans. Ind. Electron.,* vol. 61, no. 6, pp. 3071-3080, 2014.

[2] A. Chiba, T. Fukao, O. Ichikawa *et al.*, *Magnetic bearings and bearingless drives*: Elsevier, 2005, pp. Introduction.

[3] T. Baumgartner, R. M. Burkart, and J. W. Kolar, "Analysis and design of a 300-W 500 000-r/min slotless self-bearing permanent-magnet motor," *IEEE Trans. Ind. Electron.,* vol. 61, no. 8, pp. 4326-4336, 2014.

[4] P.-K. Budig, "Article to the theory and application of magnetic bearings," *in Power Electronics, Electrical Drives, Automation and Motion (SPEEDAM), 2012 International Symposium on*, Year, pp. 1526-1534.

[5] K. Inagaki, A. Chiba, M. A. Rahman *et al.*, "Performance characteristics of inset-type permanent magnet bearingless motor drives," *in 2000. IEEE, Power Engineering Society Winter Meeting*, Year, pp. 202-207.

[6] S. Kobayashi, M. Ooshima, and M. N. Uddin, "A Radial Position Control Method of Bearingless Motor Based on d-Q-Axis Current Control," *Industry Applications, IEEE Transactions on,* vol. 49, no. 4, pp. 1827-1835, 2013.

[7] X.-L. Wang, Q.-C. Zhong, Z.-Q. Deng *et al.*, "Current-controlled multiphase slice permanent magnetic bearingless motors with open-circuited phases: Fault-tolerant controllability and its verification," *IEEE Tran. Ind. Electron.,* vol. 59, no. 5, pp. 2059-2072, 2012.

[8] P. Bolognesi, "A mid-complexity analysis of long-drum-type electric machines suitable for circuital modeling," *in Electrical Machines, 2008. ICEM 2008. 18th International Conference on*, Year, pp. 1-5.

[9] Z. Zhu, Z. Xia, L. Wu *et al.*, "Analytical modeling and finite-element computation of radial vibration force in fractional-slot permanent-magnet brushless machines," *IEEE Trans. on Industry Applications,* vol. 46, no. 5, pp. 1908-1918, 2010.

[10] Z. Q. Zhu, M. Mohd Jamil, and L. Wu, "Influence of slot and pole number combinations on unbalanced magnetic force in PM machines with diametrically asymmetric windings," *IEEE Trans. on Ind. Applications,* vol. 49, no. 1, pp. 19-30, 2013.

[11] Z. Zhu, and D. Howe, "Instantaneous magnetic field distribution in brushless permanent magnet DC motors. II. Armature-reaction field," *IEEE Transactions on Magnetics,* vol. 29, no. 1, pp. 136-142, 1993.

[12] M. Ooshima, and Y. Kumakura, "Stabilized suspension control considering armature reaction in a dq axis current control bearingless motor," *in Power Electronics Conference (IPEC-Hiroshima 2014-ECCE-ASIA), 2014 International*, Year, pp. 1715-1720.

[13] P. Bolognesi, F. Papini, L. Papini *et al.*, "Effects of saturation on eccentricity force in permanent magnet synchronous machines," *in Power Electronics Electrical Drives Automation and Motion (SPEEDAM), 2010 International Symposium on*, Year, pp. 324-330.

VII. BIOGRAPHIES

Giorgio Valente received his Bachelor degree in Energy Engineering in 2011 and his Master degree in Electrical Engineering in 2014 both from the University of Padova, Italy. Between 2013 and 2014 he spent seven months at the University of Oviedo, Spain, as a visiting student, developing sensorless control techniques for PMSM for his Master thesis. He is now working towards its Ph.D. with the Power Electronics, Machines and Control Group, University of Nottingham, UK. His main research interest is control of electrical machines.

Luca Papini received his Bachelor degree (Hons.) and Master degree (Hons.) in Electrical engineering in 2009 and 2011, respectively, both from the University of Pisa, Italy. He's been visiting student at The University of Nottingham, UK, developing analytical and numerical models for his Master thesis. From June to November 2011 he collaborated with the Department of Energy Engineering, University of Pisa, as a research assistant. He is currently working towards its Ph.D. with the Power Electronic, Motors and Drives Group at University of Nottingham. Since 2013 hold a position of research assistant in the same institution.
His main research interests are high speed, high power density electric machines, machine control and levitating system.

Andrea Formentini was born in Genova, Italy, in 1985. He received the M.S. degree in computer engineering and the PhD degree in electrical engineering from the University of Genova, Genova, in 2010 and 2014 respectively. He is currently working as research fellow in the Power Electronics, Machines and Control Group, University of Nottingham. His research interests include control systems applied to electrical machine drives and power converters.

Chris Gerada (M'05) received the Ph.D. degree in numerical modeling of electrical machines from the University of Nottingham, Nottingham, U.K., in 2005. He subsequently worked as a Researcher at the University of Nottingham on high-performance electrical drives and on the design and modeling of electromagnetic actuators for aerospace applications. He was appointed as Lecturer in electrical machines in 2008, Associate Professor in 2011, and Professor in 2013. His core research interests include the design and modeling of high-performance electric drives and machines. Prof. Gerada is an Associate Editor of the IEEE Transaction on Industry Applications.

Pericle Zanchetta (M'00–SM'15) received his degree in Electronic Engineering and his Ph.D. in Electrical Engineering from the Technical University of Bari (Italy) in 1993 and 1997 respectively. In 1998 he became Assistant Professor of Power Electronics at the same University. In 2001 he became lecturer in control of power electronics systems in the PEMC research group at the University of Nottingham – UK, where he is now Professor in Control of Power Electronics systems. He has published over 200 peer reviewed papers and he is Vice-Chair of the IAS Industrial Power Converter Committee IPCC. His research interests include control of power converters and drives, Matrix and multilevel converters.